Molecular Therapy
Nucleic Acids
Original Article

A novel function and mechanism of ischemia-induced retinal astrocyte-derived exosomes for RGC apoptosis of ischemic retinopathy

Xiaoyuan Ye,[1,4] Yunfei Liu,[1,4] Congying Chen,[1,4] Yimeng Sun,[1] Fan Li,[2] Yunzhao Fu,[1] Jiawen Luo,[1] Lishi Su,[1] and Wei Chi[1,3]

[1]State Key Laboratory of Ophthalmology, Zhongshan Ophthalmic Center, Sun Yat-sen University, Guangdong Provincial Key Laboratory of Ophthalmology and Visual Science, Guangzhou 510060, China; [2]Eye Center, Zhongshan City People's Hospital, Zhongshan City, Guangdong Province 528403, China; [3]Shenzhen Eye Hospital, Guangdong Province 518000, China

Retinal ischemia is a common clinical event leading to retinal ganglion cell (RGC) death, resulting in irreversible vision loss. In the retina, glia-neuron communication is crucial for multiple functions and homeostasis. Extracellular vesicles, notably exosomes, play a critical role. The functions and mechanisms of retinal astrocyte-secreted exosomes remain unclear. Here, we isolated astrocyte-derived exosomes under hypoxia or normoxia and explored their role in an *in vivo* retinal ischemia-reperfusion (RIR) model. We found that hypoxia triggered astrocytes to produce a significantly increased number of exosomes, which could be internalized by RGCs *in vivo* or *in vitro*. Also, in the RIR model, the hypoxia-induced exosomes ameliorated the RIR injury and suppressed the RGC apoptosis. Furthermore, microRNA sequencing of retinal astrocyte-secreted exosomes revealed different patterns of exosomal miRNAs under hypoxia, particularly enriched with miR-329-5p. We verified that miR-329-5p was specifically bound to mitogen-activated protein kinase 8 mRNA, and subsequent JNK-pathway molecules were downregulated. We anticipated that the miR-329-5p/JNK pathway is a key to suppressing RGC apoptosis and preventing RIR injury. Such findings provided insights into the therapeutic potential of hypoxia-induced astrocyte-secreted exosomes and the miR-329-5p for treating retina ischemic diseases.

INTRODUCTION

Ischemic retinopathy is a common feature of many ocular diseases including acute glaucoma, diabetic retinopathy (DR), retinal vein occlusion, and retinopathy of prematurity (ROP).[1–4] Interruption of retinal blood flow is known to cause severe retinal ischemia-reperfusion (RIR) injury and retinal ganglion cell (RGC) apoptosis.[5] However, effective therapeutic strategies for RGC-damaging diseases are lacking.[6,7]

Astrocytes are among the most predominant glial cell types that, along with the vascular endothelial cells and pericytes, migrate from the brain to the retina and are mainly located in the nerve fiber layer and ganglion cell layer.[8] The astrocyte protrusions are in contact with the vessels of the superficial vascular plexus and the cytosol and axons of the RGCs.[9,10] Apart from their importance in retinal vascular development and maintenance of the blood-retina barrier, astrocytes are critical in supporting various glial homeostatic functions, such as removal of carbon dioxide, regulation of extracellular pH, intercellular transmission of intracellular signals, and the control of ionic and metabolic homeostasis in RGCs.[8,11,12] Under pathological stimuli, astrocytes will polarize and are classified as A1 (neurotoxic) or A2 (neuroprotective).[13] In models of neuroinflammation, reactive astrocytes show deleterious effects, whereas in models of ischemia, these astrocytes tend to be beneficial.[14] However, in RIR injury, both inflammation and ischemia are involved.[15] Studies conducted to date have not yet determined whether activated astrocytes contribute to the survival and axon regeneration of RGCs after ischemic retinopathy.[11,12,16–19]

Extracellular vesicles (EVs) are secreted vesicles from cells and include exosomes, microvesicles, and apoptotic bodies.[20] Exosomes are EVs of 40–160 nm in diameter generated by the endosomal pathway and carry contents including nucleic acids such as mRNA and microRNAs (miRNAs), proteins, and lipids.[21,22] During cellular communication and functional modulation, secreted exosomes can be endocytosed by recipient cells.[21]

In the past few decades, the roles of exosomes in the CNS have been explored and verified in many studies.[23,24] Exosomes from stem cells, microglia and neurons have diverse roles in neurological diseases such as stroke, Parkinson's disease (PD), and Alzheimer's disease (AD) under different conditions.[24] Naive and stimulated astrocytes shed EVs that contain neuroprotective compounds such as fibroblast growth factor 2, heat shock proteins, and miRNAs.[25] Interestingly, in

Received 18 October 2023; accepted 3 May 2024;
https://doi.org/10.1016/j.omtn.2024.102209.

[4]These authors contributed equally

Correspondence: Wei Chi, State Key Laboratory of Ophthalmology, Zhongshan Ophthalmic Center, Sun Yat-sen University, Guangdong Provincial Key Laboratory of Ophthalmology and Visual Science, Guangzhou 510060, China.
E-mail: chiwei@mail.sysu.edu.cn

certain pathological conditions like AD, PD, stroke, and other neuroinflammatory diseases, EVs released from activated astrocytes seemed to mediate or exacerbate the pathobiological course.[25] Given the key roles of astrocytes in cellular communication with other cells in the retina, retinal astrocyte-derived exosomes may be disease driving in a variety of retinal disorders. Recently, exosomes from normal mouse retinal astrocytes, rather than those from retinal pigment epithelium, were found to contain multiple anti-angiogenic factors that inhibit choroidal neovascularization (CNV) in a laser-induced CNV model.[26] Another study found that exosomes secreted by oxidative stress-induced autophagic retinal astrocytes promoted endothelial cell migration and tube formation, suggesting that these exosomes may play a neovascularizing role in ischemic-related diseases such as DR and ROP.[27] To date, the exact function, complex molecular mechanisms, and precise interaction between retinal astrocytes and RGC survival remain to be explored.

In this study, we aimed to investigate the role and effect of astrocyte-secreted exosomes stimulated in a hypoxic (hypox) or normoxic (norm) condition using the RIR model and to search for a potential therapeutic strategy for developing a treatment for ischemic retinopathy.

RESULTS

Astrocyte-derived exosome secretion increased with hypox stimulation

In the present study, we demonstrated that retinal astrocytes secreted abundant exosomes after the RIR injury compared with those under normal circumstances *in vivo* (Figures 1A–1D). We then cultured primary astrocytes including human retinal astrocytes (hACs) and mouse astrocytes (mACs) *in vitro* and extracted exosomes from cell supernatants secreted by hAC and mAC under hypox and norm conditions by ultracentrifugation and then characterized the exosomes (Figure 1E). Transmission electron microscopy (TEM) imaging revealed that exosomes secreted by hAC had a Teatro-like structure of approximately 100 nm in diameter with a clear membrane (Figure 1F). To authenticate whether the samples extracted are exosomes, exosomal contents in hAC from the norm group were extracted and purified by ultracentrifugation to discard cytoplasmic residues, and western blotting (WB) showed enriched expression of exosomal markers Flotillin, CD63, and Alix (Figure 1G). Similarly, exosomes in mACs from norm and hypox cultures analyzed with WB showed enriched expression of markers CD63, CD81, and HGS (Figure 1H).

Nanoparticle tracking analysis (NTA) was used to analyze the size and distribution of exosomes secreted from hACs and mACs. Exosomes were mostly of no more than 200 nm in diameter (Figures 1I and 1J). For hAC, the mean concentration of exosomes was approximately 6.3×10^8/mL under the norm condition and 9.9×10^8/mL in the hypox culture. For mAC, the mean concentration of exosomes was 4.6×10^8/mL in the norm culture and 7.3×10^8/mL in hypoxia (Figures 1I and 1J). Our results showed a significant increase in exosome secretion from astrocytes in hypoxia as compared with the norm condition, suggesting that hypoxia may stimulate astrocytic secretion of exosomes.

Astrocyte-derived exosomes were endocytosed by RGCs and hypoxia-induced exosomes attenuated RGC apoptosis

To investigate the influence of astrocytic exosomes on the survival of RGCs, fluorescent labeling of CD63 or PKH26 was used in *in vitro* and *in vivo* experiments, respectively. It was found that the exosomes secreted by mAC were endocytosed into RGCs (Figures 2A and 2B).

Given that RGCs endocytosed astrocyte-derived exosomes, we investigated how these exosomes would affect RGCs. Our results showed that, on day 5 after RIR injury, more RGC deaths and thinner retinas were found in the PBS group as compared with the normal control group. First, hypoxia-induced astrocyte-derived exosomes (hypox-exo) significantly decreased RGC death and retinal tissue injury compared with the norm-exo group (Figures 2C and 2D). Next, the proportion of apoptotic retinal cells was increased on day 5 of RIR injury in the PBS and norm-exo groups as compared with the normal control group, whereas the proportion of apoptotic retinal cells was significantly lower in the hypox-exo group (Figures 2E and 2F). Furthermore, the non-invasive pattern electroretinogram (PERG) was used to assess the RGC function *in vivo* and PERG suggested a neuro-protective role of hypox-exo (Figure S1). All these results suggested that hypoxia-induced astrocyte-secreted exosomes exerted a protective effect on retinal cell apoptosis from RIR injury.

miRNAs encapsulated in astrocyte exosomes induced by hypoxia differed from those under norm condition

Functional molecules such as proteins, nucleic acids, and lipids were trafficked by exosomes in cellular communication networks, and the current study, for the first time, used miRNA sequencing to investigate the exosomal miRNA content secreted by hAC. In hACs, miRNA expression was similar between the hypox and norm groups, with 12 upregulated and 17 downregulated miRNAs in the hypoxia-treated hACs (Figures 3A and 3B). However, the exosomal miRNA expressions secreted by hACs between the two groups were significantly diverse: there were 67 upregulated miRNAs and 105 downregulated miRNAs in the hypox-exo (Figures 3C and 3D). The target genes of the upregulated differentially expressed miRNAs from hypoxia-induced hAC exosomes were analyzed by Gene Ontology (GO) functional and Kyoto Encyclopedia of Genes and Genomes (KEGG) pathway annotation. GO analysis showed that the target genes were enriched in neuronal projection development, cytosolic functions of neuronal cells, and synapses between neurons (Figure 3E); KEGG analysis indicated that the target genes were involved in herpes simplex virus type 1 infection, mitogen-activated protein kinase (MAPK) signaling pathway, and PI3K-Akt signaling pathway (Figure 3F).

miR-329-5p enriched in hypoxia-induced exosomes decreased RIR injury by suppressing the apoptotic MAPK pathway

Among the upregulated differentially expressed miRNAs with the highest fold-changes in hypoxia-induced hACs (after 24 h hypoxia),

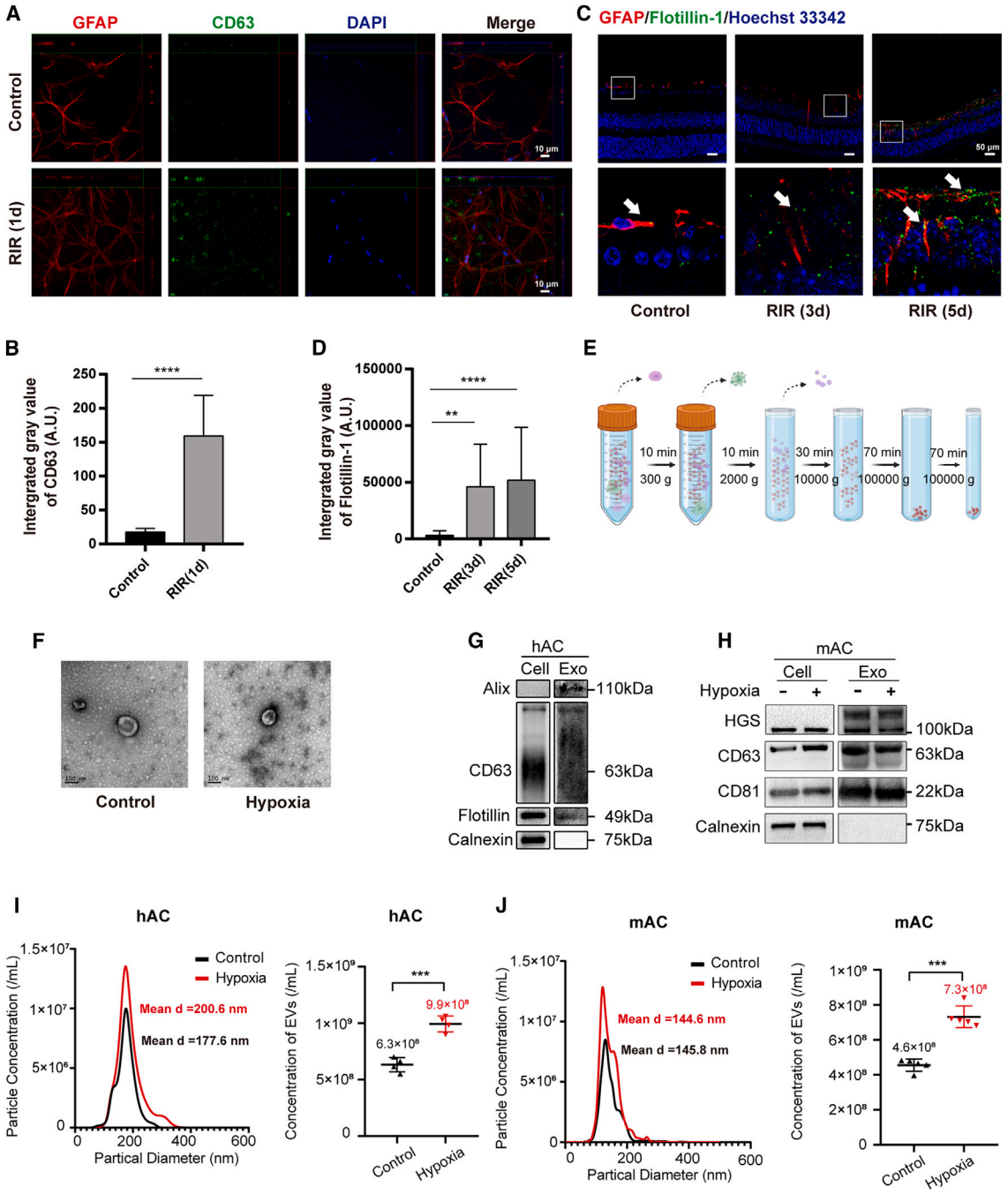

Figure 1. Increased secretion of exosomes in astrocytes after ischemic retinopathy *in vivo* or hypox stimulation *in vitro*

(A) Retinal flat mounts from mice (1 day after RIR injury) were stained for GFAP (red), CD63 (green) and DAPI (blue) and examined by confocal microscopy. (n = 3 animals; scale bar, 10 μm.) (B) Quantitative analysis of the relative fluorescence area of exosome positive protein marker CD63. (C) Representative images of immunofluorescent retinal sections of control eyes or eyes 3 or 5 days after RIR injury. (n = 3 animals; scale bar, 50 μm). (D) Quantitative analysis of the relative fluorescence area of exosome positive protein marker Flotillin. (E) Diagram showing the procedure of isolating exosomes from primary astrocytes derived supernatant using differential centrifugation. (F) TEM imaging of the morphology of exosomes secreted by hACs cultured under normoxia (Control) and 24-h hypoxia conditions (Hypoxia). (G) WB analysis of hAC cell lysates (Cell) and exo isolated from the supernatant. (H) WB analysis of cell lysates of mouse retinal astrocytes (mACs) and exosomes isolated from supernatant under normoxia or 24-h hypoxia conditions. (I and J) The distribution of particle size was analyzed through NTA (left) and statistical plots of particle concentrations (right) of hAC and mAC exosomes from the control group and the hypoxia-cultured group. Data were expressed as mean ± SD. Statistical analysis was performed using Student's *t* test. Statistical significance at $^{**}p < 0.01$; $^{***}p < 0.001$; $^{****}p < 0.0001$.

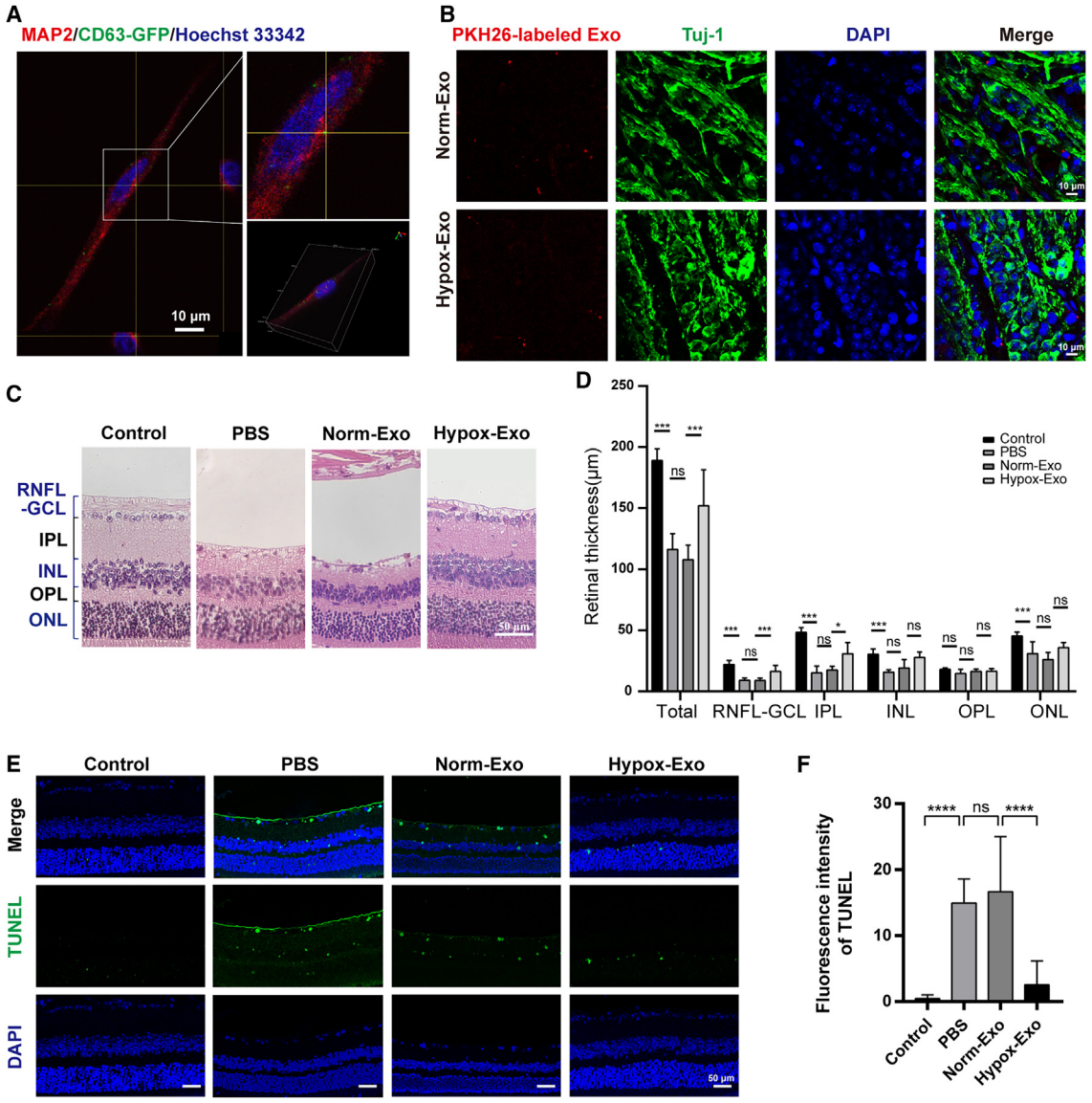

Figure 2. Astrocyte-secreted exosomes internalized by RGCs and protected the retina from ischemia-reperfusion injury

(A) 3D-fluorescent imaging of *in vitro* CD63-GFP-labeled exosomes being taken up intracellularly by RGCs. The intersection showed a CD63-GFP-labeled exosome, and the z stack side view of the x- and y axes were shown below and to the right (scale bar, 10 μm). (B) Fluorescent imaging of mouse retina flat mounts showed *in vivo* delivery of normoxia- and hypoxia-induced PKH26 labeled exosomes into retinal cells (n = 3 animals; scale bar, 10 μm). (C) HE staining and (D) comparison of retinal thickness between different treatments, at approximately 1 mm adjacent to the optic disc (n = 5 animals; scale bar, 50 μm). (E) TUNEL staining and (F) quantitative analysis of TUNEL fluorescence intensity showed apoptotic cells in retinal tissue 5 days after RIR injury (n = 5 animals; scale bar, 50 μm). Data were presented as mean ± SD. Control, normal control group; PBS, intravitreal injection of PBS; norm-exo, intravitreal injection of mAC-secreted exosomes under norm culture condition; hypox-exo, intravitreal injection of mAC-secreted exosomes under hypox culture condition; RNFL-GCL, retinal nerve fiber layer and ganglion cell layer complex; IPL, inner plexiform layer; INL, inner nuclear layer; OPL, outer plexiform layer; ONL, outer nuclear layer. Statistical significance at $^{*}p < 0.05$; $^{***}p < 0.001$; $^{****}p < 0.0001$; ns, not statistically significant.

the top three were hsa-miR-3180-5p, hsa-miR-329-5p, and hsa-miR-331-5p. However, when we conducted real-time qPCR to validate the expression levels of the top 30 miRNAs ($p < 10^{-5}$) identified in the sequencing data, some miRNAs, including miR-3180-5p, were not detectable in hypoxia-induced hAC-exo (Figure 3G). Our study further investigated the expression level of the top four miRNAs in exosomes secreted by mACs and confirmed miR-329-5p as the most abundant (Figure 3H). Furthermore, the expression of miR-329-5p in the hypoxia-induced mAC-exo increased as the hypoxia duration increased (Figure S2). To explore the effect of miR-329-5p in RIR injury, we delivered miR-329-5p agomir to ischemic-treated mice by intravitreal injection, and harvested eyes on days 0.5, 1, 3,

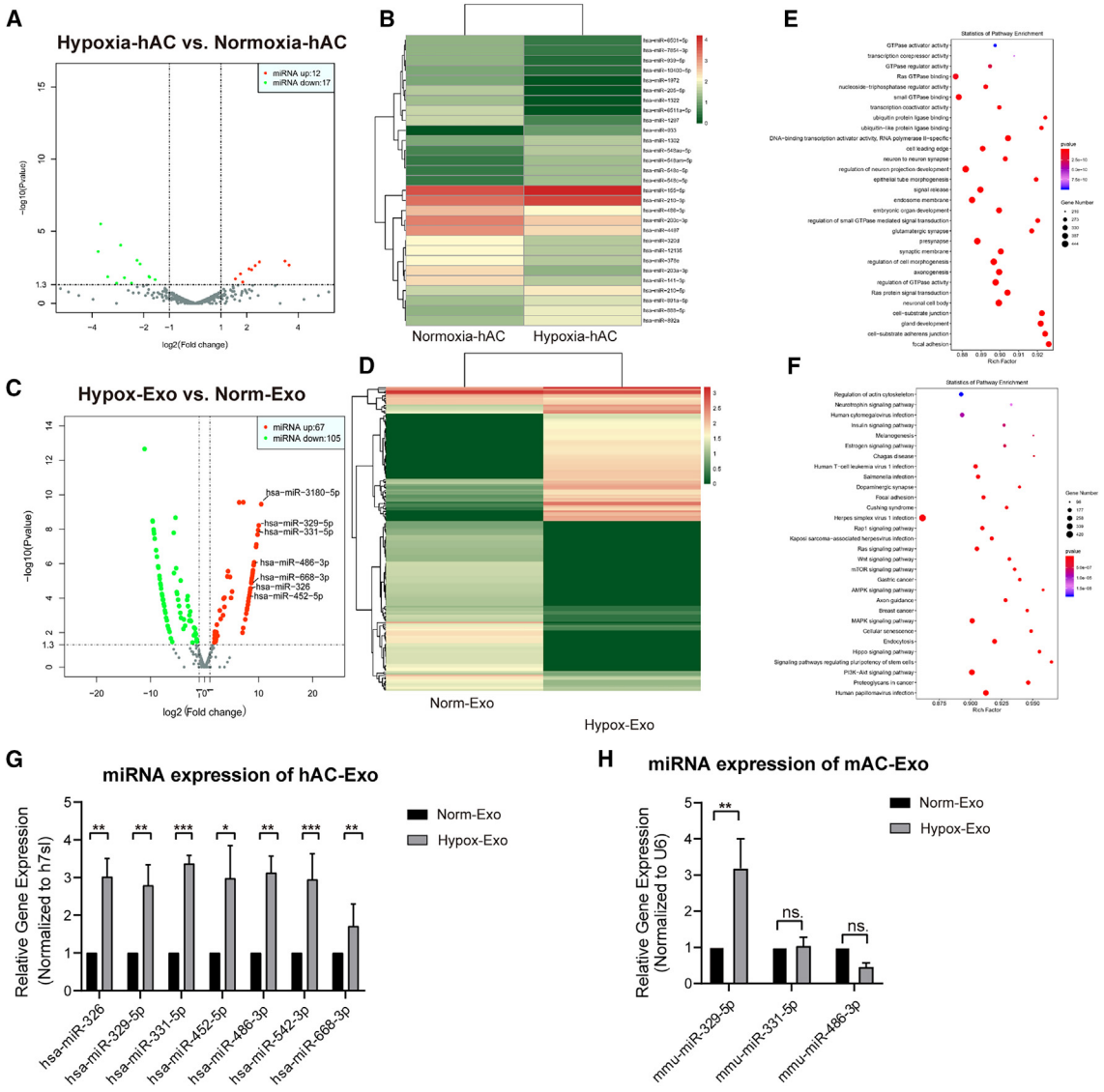

Figure 3. miRNA sequencing and bioinformatic analysis on miRNAs

(A) The volcano plot and (B) heatmap of differentially expressed miRNAs compared between hAC cultured under 24-h hypoxia (Hypoxia-hAC) and those cultured in normal condition (Normoxia-hAC). (C) Volcano plot and (D) heatmap of differentially expressed exosomal miRNAs compared between exosomes secreted by hAC cultured under 24-h hypoxia (hypox-exo) and those cultured in normal condition (norm-exo). (E) Bubble plots of GO analysis and (F) KEGG pathway of candidate target genes for possible functions and pathways. (G) Real-time qPCR analysis of various exosomal miRNAs secreted by hACs and (H) mACs cultured under 24 h of hypox condition (hypox-exo) or normal condition (norm-exo). Data were presented as mean ± SD. Statistical significance at $^{*}p < 0.05$; $^{**}p < 0.01$;$^{***}p < 0.001$;ns, not statistically significant.

and 5 after reperfusion. The retinal cryosection sections revealed that the miR-329-5p has been successfully taken up by RGCs 12 h after RIR injury (Figure S3A). Moreover, the expression of miR-329-5p was also upregulated in retina tissues of RIR mice (Figure 4A). Furthermore, histological findings demonstrated a protective effect of miR-329-5p on the ischemic retina (Figures 4B and 4C). The number of Rbpms^{+} RGCs was restored with the treatment of miR-329-5p 5 days after RIR (Figures 4D and 4E). It markedly decreased the proportion of apoptotic retinal cells, including the RGCs (Figures 4F and 4G). In addition, our study also discovered that miR-329-5p could alleviate the activation of microglia but not Müller cells (Figures S3B–S3D).

The mechanism by which miR-329-5p exerted a protective effect on the retina from IR injury was investigated by searching for target genes of hsa-miR-329-5p and mmu-miR-329-5p with databases miRDB, miRWalk, and TargetScan, and *MAPK8* was identified to be a potential target (Figures 5A and 5B). *MAPK8* encodes for

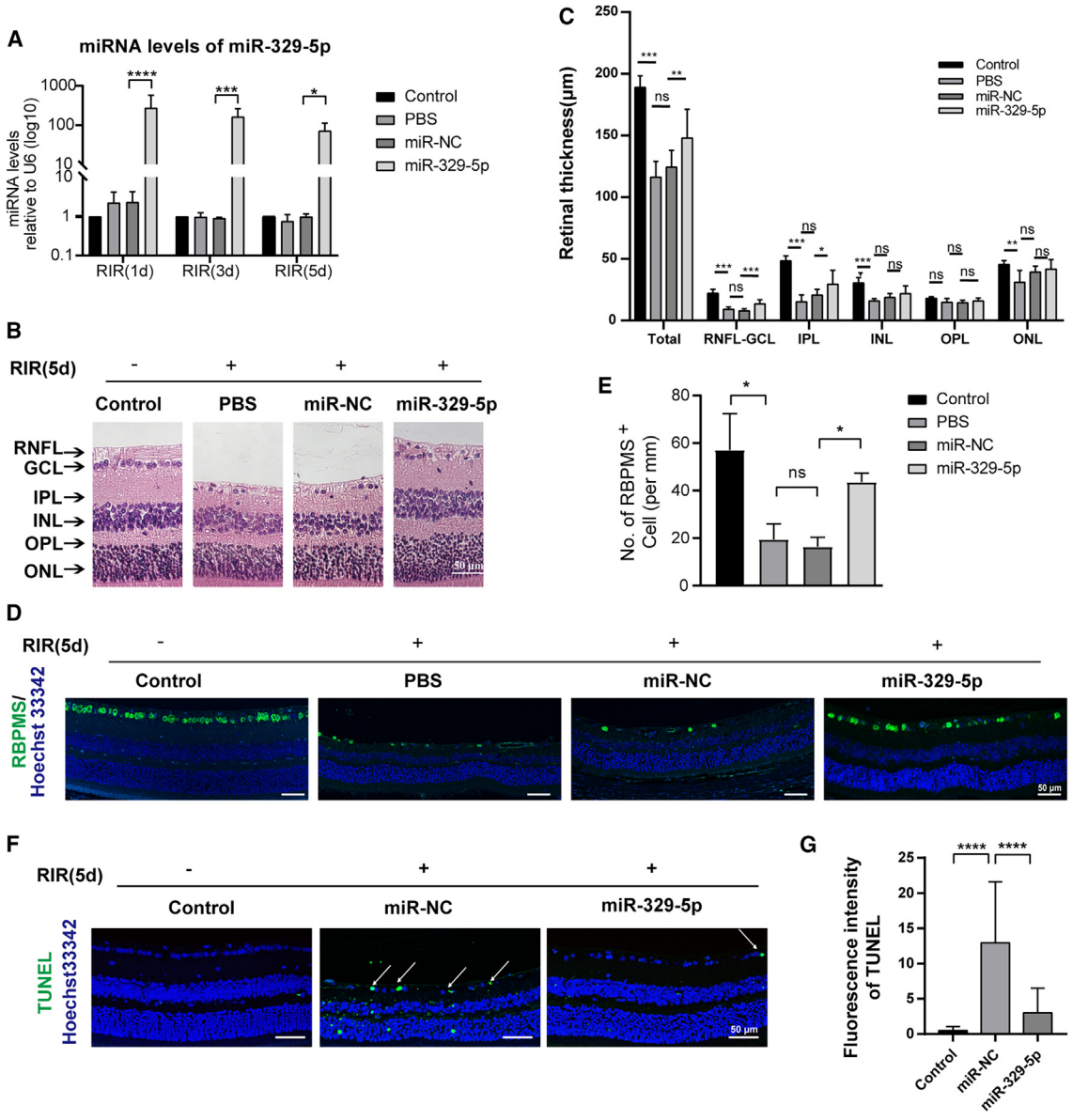

Figure 4. Effects of intravitreally injected miR-329-5p on the retina in ischemic-reperfusion injury

(A) Detection for endocytosed miRNAs in the retina by real-time qPCR after intravitreal injections of PBS or a scramble sequence of miRNA (miR-NC) or miR-329-5p agomir. (B) Retinal HE staining and (C) comparison of retinal thickness at approximately 1 mm adjacent to the optic disc among different intravitreal treatments (n = 5 animals). (D) Immunofluorescent staining with Hoechst 33342 (blue) and RBPMS (green) and (E) comparison showing the numbers of RGCs on day 5 after RIR injury (n = 5 animals). (F) TUNEL staining and (G) quantitative analysis of TUNEL fluorescence intensity to show apoptotic cells in retinal tissue on day 5 after RIR injury, with white arrows indicating apoptosis in the ganglion cell layer (n = 5). Data are expressed as mean ± SD. Data were analyzed using Student's t test or one-way ANOVA. Statistical significance was considered at $^{*}p < 0.05$; $^{**}p < 0.01$; $^{***}p < 0.001$; $^{****}p < 0.0001$. ns, not statistically significant. Scale bar, 50 μm. Control, normal control group (naive condition without any treatment); PBS, intravitreal injection of PBS; RNFL-GCL, retinal nerve fiber layer and ganglion cell layer complex; IPL, inner plexiform layer; INL, inner nuclear layer; OPL, outer plexiform layer; ONL, outer nuclear layer.

MAPK8, also known as c-Jun N-terminal kinase 1 (JNK1). MAPK8 is an important molecule in the JNK signaling, which is one route of the MAPK cascade involved with cell proliferation, survival, cell death, and differentiation.[28] Quantification of *MAPK8* mRNA and its protein expression as well as the immunohistochemistry (IHC) were performed on the eye tissues harvested 1–5 days after miR-329-5p treatment in RIR mice, and they were significantly lower than those without miR-329-5p treatment (Figures 5C–5F). Meanwhile, immunoblotting results indicated that miR-329-5p treatment downregulated protein expression levels of *p*-MAPK8, c-JUN, Bax, and cleaved

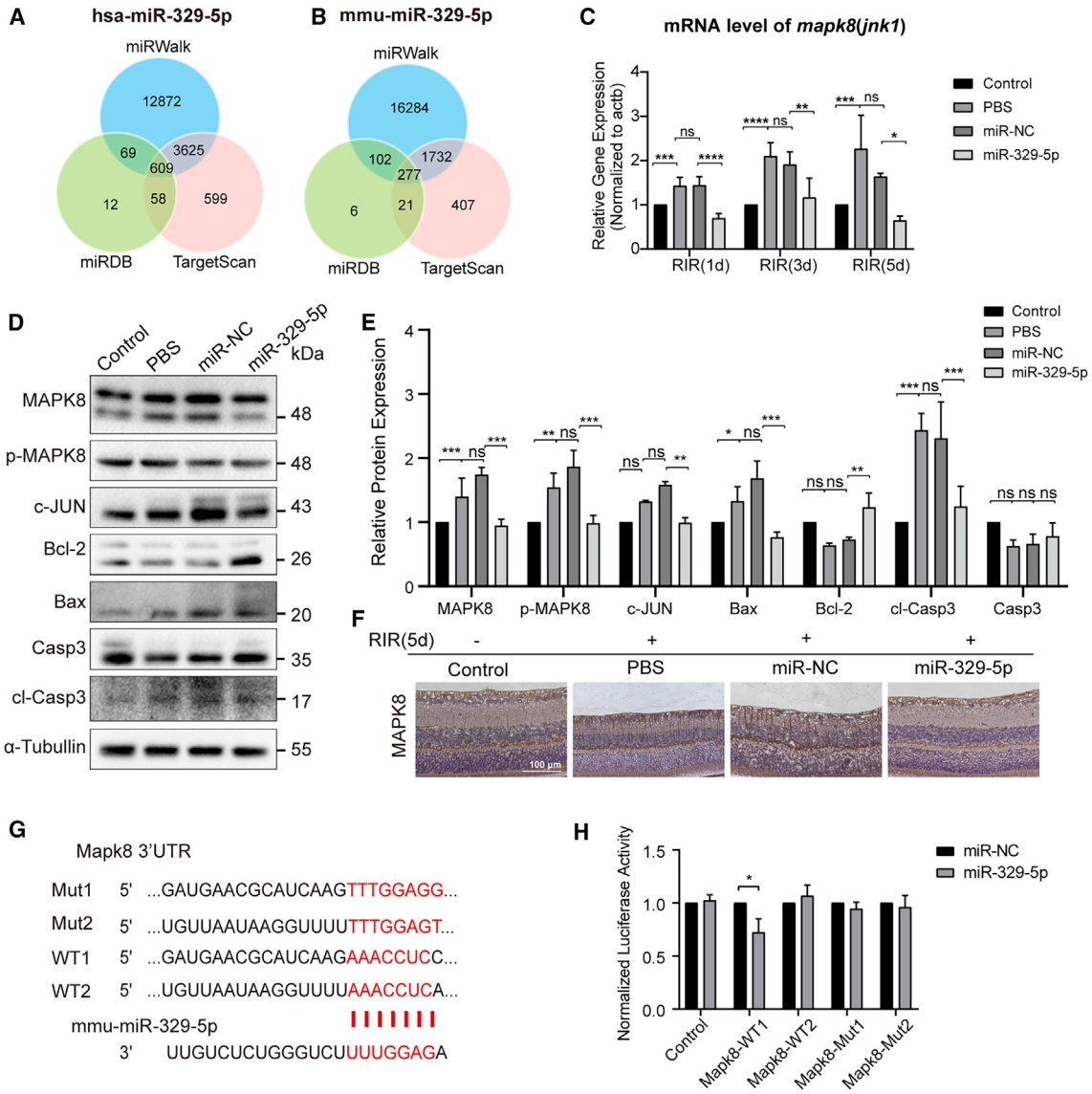

Figure 5. miR-329-5p protected the retina from ischemic-reperfusion injury by targeting the MAPK pathway

(A and B) Venn diagrams showing the intersection of predicted target genes of hsa-miR-329-5p and mmu-miR-329-5p, and *MAPK8* (Jnk1) is a potential gene targeted by both miRNAs. (C) Real-time qPCR analysis of *MAPK8* mRNA expression after intravitreal treatment of PBS, scrambled miRNA (miR-NC), and miR-329-5p (n = 5). (D and E) WB and quantification of protein expressions of *MAPK8*-related pathway on retinal tissues after intravitreal treatments of PBS, miR-NC, and miR-329-5p (n = 5). (F) IHC of MAPK8 expression on retinal tissues after various intravitreal treatments (n = 5 animals; scale bar, 100 μm). (G) Dual-luciferase reporter gene plasmid design and the predicted target sites. (H) The dual luciferase reporter gene assay showed that miR-329-5p significantly inhibited the luciferase activity of the *MAPK8*-WT1 3′UTR reporter gene in 293T cells. Data was presented as mean ± SD, n = 3. Student's t test was used for statistical analysis. Data were statistically analyzed by one-way ANOVA followed by Tukey's post hoc analysis. Statistical significance at $^{*}p < 0.05$; $^{**}p < 0.01$; $^{***}p < 0.001$; $^{****}p < 0.0001$. ns, not statistically significant.

caspase3 while enhancing the expression level of Bcl-2 (Figures 5D and 5E), suggesting that miR-329-5p may inhibit apoptosis by suppressing the MAPK signaling pathway. To verify whether miR-329-5p specifically targeted *MAPK8* mRNA, we designed wild-type and mutant plasmids of MAPK8 (Figure 5G) and co-transfected them with miR-329-5p mimics in 293T cells and found that the miRNA mimics significantly decreased the luminescence intensity of *MAPK8*-WT1, suggesting that miR-329-5p specifically targeted the binding site of *MAPK8*-WT1 (Figure 5H)

DISCUSSION

RIR injury is a recognized common pathological process in a wide range of ocular diseases, such as glaucoma, DR, retinal vein occlusion, retinal artery occlusion, and ROP.[29] The injury can lead to RGC

damage or loss, resulting in impaired visual function or even blindness. The damage to the retina is irreversible. Currently, there are no effective drugs to treat nerve cell injury. By using the acute high intraocular pressure (IOP) model, a classic RIR model, we explored and found the protective role of hypoxia-induced astrocyte (hAC)-derived exosomes on retinal cells, and for the first time, we discovered that miR-329-5p was enriched in exosomes under ischemic conditions and protected retinal impairment by targeting the JNK signaling pathway.

Exosomes are a subtype of EVs formed by an endosomal route and are responsible for trafficking and endocytosis of cellular materials during cell-cell communications involved in various biological processes.[30] In the CNS, the mechanisms of astrocytic exosome biogenesis and secretion and their possible functional interactions with target cells have been extensively studied.[23,25] The effect of astrocyte-derived exosomes on the CNS varies depending on their astroglia types (A1 or A2) or contents. For instance, those astrocyte-derived exosomes enriched in synapsin-1 or miR-26a are beneficial, whereas those containing miR-125a-5p and miR-16-5p are detrimental.[25,31] However, the role of astrocytic exosomes in RIR is not well explored. The current study revealed that under the hypox condition in the RIR model, activated astrocytes secreted exosomes could be endocytosed by RGCs, and RGC apoptosis was decreased, thus protecting retinal cells from ischemic damage.

Exosomes have several inherent characteristics, such as antigen-presenting vesicles with a long half-life, which enables them to be well tolerated by the human body. Moreover, the ability to load both proteins and genetic materials makes them attractive and ideal for the development of a drug-delivery system.[22,32,33] The various encapsulated components (nucleotides, lipids and proteins) enable exosomes to serve as potential versatile treatments for diseases. miRNAs are one type of nucleotides that have the potential to regulate and alter protein expression, signaling pathways, and molecular mechanisms. In the RIR model, it has been shown that miRNAs are involved in regulating the pathology of RIR injury.[34] Li et al.[35] demonstrated that co-delivery of miRNA-124 and brinzolamide through bio-degradable nanoparticles for glaucoma treatment could achieve synergistic therapeutic effects. Yet, exosomal miRNAs in retinal injury models were understudied. The specificity of miRNAs in exosomes is determined by a certain RNA sorting mechanism and varies from different stimuli.[36,37] In the present study, in response to RIR, stimulated miRNAs were transmitted to RGCs by endocytic cargo as secreted exosomes from astrocytes, suggesting the potential of exosomes to act as therapeutic vehicles for retinal ischemic diseases. By bioinformatic analysis and screening, we found that miR-329-5p was enriched in hypoxia-activated astrocyte-secreted exosomes, implying that this miRNA may be an important player that contributed to the protection of RGCs from ischemic damage.

It is of interest to study the underlying signaling pathway and mechanism by which miR-329-5p exerted inhibitory regulation on RGC apoptosis. Further analysis of its potential binding sites revealed that miR-329-5p may target and suppress *MAPK8* expression, and subsequently downregulating the JNK pathway. *MAPK8*, also known as JNK1, is a JNK protein isoform broadly expressed in various cell types and is involved in the JNK pathway of the MAPK cascade. *MAPK8* is responsible for the regulation of cell proliferation, survival, cell death, and differentiation.[28] It has been found that JNK1 plays a key role in intrinsic programmed RGC death after axonal injury.[38] Its downstream molecule, c-JUN, is also important in RGC degeneration caused by high IOP.[39] Yang et al.[40] constructed an optic nerve injury model and demonstrated that degeneration of pathological axons in RGCs was mediated by MAPK cascades. In our study, by intraocular treatment of miR-329-5p, we found that the protein expression of JNK1 and c-JUN was suppressed, and endogenous apoptosis in retinal cells was decreased, thereby relieving RIR injury. These results elucidated the mechanism of JNK-pathway inhibition targeted by miR-329-5p. Therefore, miR-329-5p treatment may be a potential therapeutic strategy in regulating gene expression and modulating key apoptosis pathways to prevent RIR injury. The use of exosomes to encapsulate miR-329-5p might have more distinct advantages in therapeutic applications in RIR injury. Exosomes, as naturally secreted cellular vesicles, exhibit high biocompatibility and permeability and low immunogenicity.[41,42] The direct exposure of miRNA molecules to the tissue environment can lead to rapid degradation. The encapsulation within exosomes not only enriches the therapeutic components, but also significantly enhances their stability.[43] This enhancement facilitates prolonged and efficient transport from astrocytes to RGCs, potentially increasing the therapeutic efficacy of miRNA-based neuroprotective treatments. Based on these advantages, the potential for exosome engineering opens new avenues for targeted therapy in RIR. By modifying the surface molecules of exosomes, it is possible to achieve a high degree of specificity in delivering therapeutic agents to RGCs, minimizing off-target effects and maximizing therapeutic outcomes.[42,44] As research into the mechanisms of RIR injury progresses, the capacity of exosomes to carry a diverse array of therapeutic components for comprehensive treatment strategies holds promise. Therefore, further studies on miR-329-5p-engineered exosomes are needed in the future.

In conclusion, our study demonstrated that hypoxia-stimulated astrocytes secreted exosomes carrying miR-329-5p, which protected RGCs from ischemia-related apoptosis by targeting *MAPK8* and inhibited the JNK pathway. The discovery of this novel therapeutic exosomal miRNA (miR-329-5p) offers promising clinical applications for targeting the treatment of retinal ischemia-related ocular disorders such as glaucoma, retinal vein occlusion, DR, and ROP.

MATERIALS AND METHODS

Primary astrocyte isolation, culture, and hypoxia treatment

Primary mACs were isolated and cultured following previous methods.[45] Briefly, cerebral cortices without meninges and blood vessels were dissected from neonatal C57BL/6J mice (postnatal days 0–1) in Dulbecco's PBS (DPBS, Gibco, Thermo Fisher Scientific) and digested with 0.125% trypsin for 15 min. Isolated cortical cells were suspended in DMEM (Gibco) containing 10% fetal bovine serum (FBS,

Gibco) and plated at a density of 6×10^5 cells/cm^2 on uncoated 25 cm^2 flasks. Astrocytes were harvested 11–12 days after purifying by shaking the flask and were dissociated by trypsinization and then reseeded on culture dishes. After cells reached 70%–80% confluence, the culture medium was changed to DMEM containing 10% exosome-free FBS, which was prepared by ultracentrifugation at 100,000×*g* for 16 h at 4°C before use.[46]

For the hypox culture condition, astrocytes were incubated with 1% oxygen in a Hypoxystation (HypoxyLab, Oxford Optronix); otherwise, astrocytes were cultured at a normal level of oxygen in an incubator (norm condition). The supernatant was collected 24 h after the oxygen level change.

Cell culture: Primary RGCs and other cell lines

Primary RGCs were isolated from neonatal C57Bl/6J mice (postnatal days 0–1) using the Papain Dissociation System (Worthington Biochem) as previously described.[47] After isolation, primary RGCs were cultured in Neurobasal-A medium (Gibco) containing 2% B27 (Gibco) and 1% glutamine.

hACs were purchased from ScienCell Research Laboratories. hACs were cultured with the standard protocol using Astrocyte Medium (ScienCell, Cat. No.1801), supplemented with 2% exosome-free FBS, 1% astrocyte growth supplement, and 1% penicillin/streptomycin solution. The 293T cell line was purchased from the American Type Culture Collection (ATCC) with DMEM containing 10% FBS.

Animal model of retinal ischemic injury

Adult male C57BL/6J mice were purchased from the Model Animal Research Center at Nanjing University. The retinal ischemic injury model was established as previously described.[48] First, mice were anesthetized with 100 mg/kg pentobarbital sodium intraperitoneally, and 0.5% proparacaine (SomnoSuite; Kent Scientific) was applied topically. Pupils were dilated using 1% tropicamide. Ischemia in the retina was achieved by increasing IOP: insertion of a 30G needle (BD) connecting to a normal saline reservoir in the anterior chamber and cannulation was made to elevate and maintain at an average IOP of 110 mm Hg for 60 min. The contralateral eye served as the sham group without elevated IOP. Retinal ischemia was confirmed with the absence of the red light reflex in the fundus, conjunctival edema, and corneal haze, whereas the recovery of the red light reflex indicated subsequent reperfusion. To prevent infection, the eyes were treated with tobramycin ointment. This study excluded eyes with cannulation-induced cataracts, iris injury and/or bleeding, or anterior chamber leakage.

After the withdrawal of the needle from the anterior chamber, each experimental eye was intravitreally injected with PBS, negative control miRNA (miR-NC) (20 μM/2 μL), mmu-miR-329-5p agomiR (miR-329-5p), the Cy5-labeled mmu-miR-329-5p agomiR (RiboBio), or exosomes released either from normoxia (norm-exo) or hypoxia (hypox-exo) treated astrocytes. The mice were sacrificed on days 0.5, 1, 2, 3, or 5 after intravitreal injection, and enucleated eyeballs were harvested.

Exosome purification and analysis

Exosomes were isolated from the astrocyte-conditioned medium by differential centrifugation following the previously described protocol.[49] Briefly, the medium was collected, centrifuged at 300×*g* for 10 min and 2,000×*g* for 10 min to eliminate cell debris, and at 10,000×*g* for 30 min to eliminate large EVs, followed by filtration through a 0.22-μm micro-filter. Exosomes were pelleted by ultracentrifugation at 100,000×*g* for 70 min, and the pellet was washed with PBS before final ultracentrifugation at 100,000×*g* for 70 min. All centrifugation steps were conducted at 4°C.

TEM assay

A TEM assay was performed for the observation of the exosome samples. The TEM assay was commissioned to OBiO Technology Corp., Ltd.

NTA

The number and sizes of exosomes were tracked using the Nanosight NS 300 system (NanoSight Technology). The exosome pellet isolated from 90 mL supernatant was re-suspended in PBS. Samples were manually injected into the sample chamber. Exosome sizes were measured at a camera setting with an acquisition time of 40 s for 4 times per sample and a detection threshold of 5. The NTA analytical software version 2.3 was used for capturing images and analyzing the data.

Exosome tracing *in vitro* and *in vivo*

The CD63-GFP plasmid was extracted from the CD63 plasmid strain (Addgene) and then transfected into mAC using the Lipofectamine 3000 transfection kit (Cat. No. L3000-15, Invitrogen). After 8 h of transfection, cells were cultured for 24 h using DMEM containing 10% exosome-free FBS. CD63-GFP-labeled exosomes were collected and added to the supernatant of primary RGCs. After 24-h incubation, cells were fixed with 4% paraformaldehyde for 30 min and treated with 0.2% Triton X-100 (Sigma-Aldrich, St. Louis) at the ambient temperature for 10 min. Cells were incubated with anti-MAP2 primary body overnight followed by 1-h incubation with Alexa Fluor 549 Conjugate (Invitrogen). Hoechst 33342 (5 μg/mL, Sigma-Aldrich) was used for nuclear counterstaining.

For *in vivo* experiments, norm-exo and hypox-exo were collected from primary astrocyte media and labeled with PKH26 (Sigma-Aldrich). The PKH26-labeled exosomes were injected into the vitreous cavity of mice and the eyeballs were collected after 24 h. Whole retina flat mounts were prepared and co-stained with Tuj1 and DAPI (Beyotime). Fluorescent images were captured with a Nikon A1 Spectral Confocal Microscope or Zeiss LSM 880 with Airyscan.

miRNA sequencing

miRNA sequencing was commissioned to RiboBio. miRNA sequencing of exosomes (from hypoxia and normoxia cultured

Table 1. Antibodies used in this study

Name	Product catalog
Alexa Fluor 488 Conjugate	Invitrogen
Alexa Fluor 549 Conjugate	Invitrogen
Anti-Alix rabbit pAb	Novus, Cat#. NBP1-90201
Anti-Bax rabbit Ab	Cell signaling, Cat#. 2772s
Anti-Bcl-2 rabbit mAb	Cell signaling, Cat#. 2870s
Anti-Calnexin rabbit pAb	Abcam, Cat#. ab22595
Anti-CD63 rabbit mAb	Abcam, Cat#. ab217345
Anti-CD63 rabbit pAb	System Biosciences, Cat#. EXOAB-CD63A-1
Anti-CD81 rabbit mAb	Cell Signaling, Cat#. 10037s
Anti-c-JUN rabbit mAb	Cell Signaling, Cat#. 9165s
Anti-cleaved-Caspase 3	Cell Signaling, Cat#. 9661s
Anti-Flotillin-1 rabbit mAb	Cell Signaling, Cat#. 18634s
Anti-GFAP mouse mAb	Cell Signaling, Cat#. 3670s
Anti-HGS rabbit pAb	Abcam, Cat#. 155539
Anti-HIF1α rabbit pAb	Abclonal, Cat#. A11945
Anti-Iba1 rabbit mAb	Abcam, Cat#. ab178847
Anti-JNK1 rabbit pAb	Huabio, Cat#. R1309-1
Anti-MAP2 rabbit pAb	Invitrogen, Cat#. PA5-110744
Anti-*p*-JNK1 (Thr183/Tyr185) rabbit pAb	Abcepta, Cat#. AP22143a
Anti-RBPMS rabbit pAb	Abcam, Cat#.152101
Anti-α-Tubulin antibody	Arigobio, Cat#. ARG65693
Anti-β-Actin rabbit mAb	Cell Signaling, Cat#. 4970s
Anti-β-III-Tubulin mouse mAb	Abcam, Cat#. Ab78078
Goat anti-Mouse IgG antibody (HRP)	Arigobio, Cat#. ARG65350
Goat anti-Rabbit IgG antibody (HRP)	Arigobio, Ca#. ARG65351

astrocyte media) and astrocytes was performed using the Illumina HiSeqTM 2500. Relative sequencing data in this study can be found at Gene Expression Omnibus: GSE266311.

Histological evaluation and IHC

Staining for hematoxylin and eosin (HE, Nanjing Jiancheng Technology Ltd.) and IHC (Abcam, ab80436) was performed on 5-μm-thick paraffined sections with finely adjusted standard protocols or manufacturer's instructions. Briefly, sections were first deparaffinized and rehydrated using a series of xylene and ethanol solutions. For HE staining, the sections were stained with hematoxylin solution, followed by rinsing with tap water, and then counterstained with eosin solution. For IHC staining, the slices were treated with 3% hydrogen peroxide for 15 min, followed by antigen retrieval by heating the sections in a citrate buffer solution for 20 min. The samples were then incubated with primary antibodies in an antibody diluent agent (DAKO, S3022) overnight at 4°C. After washing with PBS, chromogen, 3,3′-diaminobenzidine was added to visualize the target antigens and hematoxylin was counterstained to visualize the nucleus. The sections were then dehydrated using ethanol, cleared in xylene, and mounted with coverslips. Images of the slices were captured using an inverted microscope (Eclipse Ti-U).

Immunofluorescence staining and TUNEL

Immunofluorescence (IF) staining was performed in paraffined sections, retinal flat mounts, and cryosections in this study. Paraffined sections were deparaffinized and rehydrated and went through the antigen retrieval process as mentioned earlier. Flat-mounted retinae and eyeball cryosections were prepared as previously described.[6,50] The samples were incubated with the indicated primary antibodies overnight and then the fluorescence-conjugated secondary antibodies (Molecular Probes, Thermo Fisher Scientific) for 1 h. Then, the samples were washed using PBS and stained with Hoechst 33342 or DAPI for 10 min. The film was sealed with a water-soluble sealing agent.

TUNEL was performed on paraffined sections based on the instructions. Briefly, the sections were deparaffinized, rehydrated, and treated with proteinase K. Sections were then stained with a TUNEL reaction mixture containing fluorescein-labeled dUTP (TUNEL, In Situ Cell Death Detection Kit, Roche) followed by DAPI.

All images were captured with the confocal microscope (Nikon A1 Spectral Confocal Microscope, or Zeiss LSM 880 with Airyscan). Antibodies for IHC and IF are listed in Table 1.

WB

Total protein lysates were extracted from cells, isolated exosomes, or retina tissues and processed for assessing protein expression levels. Extracted protein lysates were assessed with general WB protocol for expression of Calnexin, Flotillin, CD63, CD81, Alix, HGS, α-tubullin, caspase-3, cleaved caspase-3, Bax, Bcl-2, c-JUN, MAPK8, and phosphorylated JNK1. Selected antibodies are listed in Table 1.

RNA isolation and real-time qPCR

Exosomal RNA was extracted using a *SeraMir* Exosome RNA Amplification Kit (System Biosciences,). Total RNA from tissue was extracted with TRIzol reagent (Thermo Fisher Scientific) according to the manufacturer's standard procedure, followed by reverse transcription and real-time qPCR.[51] In this study, we followed the method established by Schmittgen and Livak[52] on relative gene expression (classical ΔΔCt method). The primers of the target genes are listed in Table 2 and Table 3.

Luciferase reporter assay

To determine the binding sites of miR-329-5p on *MAPK8*, a luciferase reporter assay was performed. 293T cells were transfected with a dual-Luciferase construct containing *MAPK8* of wild-type or with a mutation at the binding site. The cells were co-transfected with miR-329-5p and miR-NC using Lipofectamine 3000 (Invitrogen). After 6 h, the medium was replaced, and after 24 h, the luciferase activities were confirmed using a Dual-Luciferase kit (GeneCopoeia).

Table 2. Reverse transcription sequences used in real-time qPCR test

miRNA name	Reverse transcription sequence (5′-3′)
h7sl	CAGCACGGGAGTTTTGACCT
hsa-miR-326	CTCAACTGGTGTCGTGGAGTCGGCA ATTCAGTTGAGCTGGAGGA
hsa-miR-329-5p	CTCAACTGGTGTCGTGGAGTCGGCA ATTCAGTTGAGGAAACAGA
hsa-miR-331-5p	CTCAACTGGTGTCGTGGAGTCGGCA ATTCAGTTGAGGGATCCCT
hsa-miR-452-3p	CTCAACTGGTGTCGTGGAGTCGGCAA TTCAGTTGAGTCAGTTTC
hsa-miR-486-3p	CTCAACTGGTGTCGTGGAGTCGGCAA TTCAGTTGAGATCCTGTA
hsa-miR-542-3p	CTCAACTGGTGTCGTGGAGTCGGCAA TTCAGTTGAGTTTCAGTT
hsa-miR-668-3p	CTCAACTGGTGTCGTGGAGTCGGCAA TTCAGTTGAGGTAGTGGG
U6	ACGCTTCACGAATTTGCGTGTC
mmu-miR-329-5p	CTCAACTGGTGTCGTGGAGTCGGCAA TTCAGTTGAGAACAGAGA
mmu-miR-331-5p	CTCAACTGGTGTCGTGGAGTCGGCA ATTCAGTTGAGGGATCCCT
mmu-miR-486-3p	CTCAACTGGTGTCGTGGAGTCGGCAA TTCAGTTGAGATCCTGTA

PERG

The recording electrodes were made of thin silver wire (0.25 mm in diameter) wound into semicircular rings with a radius of 2 mm. The electrodes for the right and left eyes had a mirrored geometry, with the vertical part of the electrode connected to the electrode holder located on the temporal side of the eye so as not to interfere with vision. Electrode positioning required minimal manipulation of the eye. The reference electrode and ground electrode were small stainless steel needles inserted into the skin near the eye and tail, respectively. The anesthetized mice were fixed on the scaffolds and the corneal electrodes were placed on the right or left eye, with the body temperature maintained at 35°C. Artificial tears were administered every 30 min to keep the cornea and lens in good condition during the recording period (approximately 1 h).

PERG was obtained by contrast inversion in response to patterned visual stimuli (horizontal grating, vertical grating, checkerboard), rather than uniform flashes. To maximize PERG amplitude, the patterned visual stimulus was, therefore, a horizontal grating with high contrast (98%), a spatial frequency of 0.05 cyc/deg with a square wave profile, a spatial phase with a sudden frequency of 1 Hz (two contrast inversions/second) and 150 cd/m^2 average brightness. The stimulus was generated by a video card and displayed on a 21-inch TV monitor. To further maximize PERG amplitude, a large stimulus area (84.8° × 80.0°) was obtained by presenting the patterned stimulus from a short distance (18 cm). The stimulus display contained four complete stimulus cycles. The center of the visual stimulus was aligned with the pupil projection. The PERG responses were superimposed to check consistency and then averaged (100 cycles).

Statistics

Data were presented as the mean ± SD. One-way ANOVA followed by Bonferroni multiple comparison tests was used to compare three or more groups, and two-tailed unpaired t tests were used to compare two groups. Statistical analysis was performed with GraphPad Prism software (version 8.0, GraphPad Software, Inc., San Diego, CA, USA). p values of less than 0.05 were considered to indicate statistical significance.

Table 3. Primer sequences used in real-time qPCR test

Gene/miRNA name	Forward primer sequence (5′-3′)	Reverse primer sequence (5′-3′)
h7sl	ATCGGGTGTCCGCACTAAGTT	CAGCACGGGAGTTTTGACCT
hsa-miR-326	ACACTCCAGCTCAGCCTCTGGGCCCTTCCTC	CTCAACTGGTGTCGTGGAGTCGGCAATTCAG
hsa-miR-329-5p	ACACTCCAGCTCAGGAGGTTTTCTGGGTTTC	CTCAACTGGTGTCGTGGAGTCGGCAATTCAG
hsa-miR-331-5p	ACACTCCAGCTCAGCTAGGTATGGTCCCAGG	CTCAACTGGTGTCGTGGAGTCGGCAATTCAG
hsa-miR-452-3p	ACACTCCAGCTCAGAACTGTTTGCAGAGGAA	CTCAACTGGTGTCGTGGAGTCGGCAATTCAG
hsa-miR-486-3p	ACACTCCAGCTCAGCGGGGCAGCTCAGTACA	CTCAACTGGTGTCGTGGAGTCGGCAATTCAG
hsa-miR-542-3p	ACACTCCAGCTCAGTGTGACAGATTGATAAC	CTCAACTGGTGTCGTGGAGTCGGCAATTCAG
hsa-miR-668-3p	ACACTCCAGCTCAGTGTCACTCGGCTCGGCC	CTCAACTGGTGTCGTGGAGTCGGCAATTCAG
U6	CTCGCTTCGGCAGCACATATACT	ACGCTTCACGAATTTGCGTGTC
mmu-miR-329-5p	ACACTCCAGCTCAGAGAGGTTTTCTGGGTCT	CTCAACTGGTGTCGTGGAGTCGGCAATTCAG
mmu-miR-331-5p	ACACTCCAGCTCAGCTAGGTATGGTCCCAGG	CTCAACTGGTGTCGTGGAGTCGGCAATTCAG
mmu-miR-486a-3p	ACACTCCAGCTCAGCGGGGCAGCTCAGTACA	CTCAACTGGTGTCGTGGAGTCGGCAATTCAG
actb (mouse)	GGCTGTATTCCCCTCCATCG	CCAGTTGGTAACAATGCCATGT
mapk8/jnk1 (mouse)	GTGGAATCAAGCACCTTCACT	TCCTCGCCAGTCCAAAATCAA

DATA AND CODE AVAILABILITY

The data that support the findings of this study are available from the corresponding author upon reasonable request. Relative sequencing data in this study can be found at Gene Expression Omnibus: GSE266311.

SUPPLEMENTAL INFORMATION

Supplemental information can be found online at https://doi.org/10.1016/j.omtn.2024.102209.

ACKNOWLEDGMENTS

All the animals were handled in strict accordance with Animal Research: Reporting of In Vivo Experiments (ARRIVE) guidelines, and this study was formally reviewed and approved by the Zhongshan Ophthalmic Center Animal Care and Ethics Committee (2020–015). The authors appreciate the funding that supports this study, including the National Natural Science Foundation of Key Program of China to W.C. (No. 82230031), the National Natural Science Foundation of China to W.C. (No. 82070950), the Guangzhou Key Research and Development Program, Guangzhou Municipal Science and Technology Bureau to W.C. (No. 202206010001), the Guangzhou Municipal Science and Technology Bureau City-School (Institute) Jointly Funded Project to W.C. (No. 202102010320), the Shenzhen Bay Laboratory Basic Research Program to W.C. (No. SZBL2021080601009), and the Natural Science Foundation of Guangdong Province of China to F.L. (No. 2023A1515011225). The funding organizations had no role in the design or execution of this research. The authors also thank Dr. Wei Yin and his team at Sun Yat-sen University for their kind help in offering some of the equipment needed in this study.

AUTHOR CONTRIBUTIONS

Study concept and design: W.C., Y.X., and Y.L. Experimental and technical support: W.C., X.Y., Y.L., C.C., Y.S., Y.F., and J.L. Acquisition, analysis, or interpretation of data: W.C., X.Y., Y.L., C.C., and L.S. RNA sequencing analysis: X.Y. and C.C. Drafting of the manuscript: W.C., X.Y., and Y.L. Critical revision of the manuscript for important intellectual contents: W.C., Y.X., Y.L., and F.L. Statistical analysis: W.C., X.Y., and L.S. All authors read and approved the final manuscript.

DECLARATION OF INTERESTS

The authors declare no competing interests.

REFERENCES

1. Baliño, P., Gómez-Cadenas, A., López-Malo, D., Romero, F.J., and Muriach, M. (2019). Is There A Role for Abscisic Acid, A Proven Anti-Inflammatory Agent, in the Treatment of Ischemic Retinopathies? Antioxidants *8*. https://doi.org/10.3390/antiox8040104.
2. Xu, W.Q., and Wang, Y.S. (2016). The role of Toll-like receptors in retinal ischemic diseases. Int. J. Ophthalmol. *9*, 1343–1351. https://doi.org/10.18240/ijo.2016.09.19.
3. Terelak-Borys, B., Skonieczna, K., and Grabska-Liberek, I. (2012). Ocular ischemic syndrome - a systematic review. Med. Sci. Mon. Int. Med. J. Exp. Clin. Res. *18*. Ra138–144. https://doi.org/10.12659/msm.883260.
4. Hardy, P., Beauchamp, M., Sennlaub, F., Gobeil, F., Jr., Tremblay, L., Mwaikambo, B., Lachapelle, P., and Chemtob, S. (2005). New insights into the retinal circulation: inflammatory lipid mediators in ischemic retinopathy. Prostaglandins Leukot. Essent. Fatty Acids *72*, 301–325. https://doi.org/10.1016/j.plefa.2005.02.004.
5. Nashine, S., Liu, Y., Kim, B.J., Clark, A.F., and Pang, I.H. (2014). Role of C/EBP homologous protein in retinal ganglion cell death after ischemia/reperfusion injury. Invest. Ophthalmol. Vis. Sci. *56*, 221–231. https://doi.org/10.1167/iovs.14-15447.
6. Chen, H., Deng, Y., Gan, X., Li, Y., Huang, W., Lu, L., Wei, L., Su, L., Luo, J., Zou, B., et al. (2020). NLRP12 collaborates with NLRP3 and NLRC4 to promote pyroptosis inducing ganglion cell death of acute glaucoma. Mol. Neurodegener. *15*, 26. https://doi.org/10.1186/s13024-020-00372-w.
7. Osborne, N.N., Casson, R.J., Wood, J.P.M., Chidlow, G., Graham, M., and Melena, J. (2004). Retinal ischemia: mechanisms of damage and potential therapeutic strategies. Prog. Retin. Eye Res. *23*, 91–147. https://doi.org/10.1016/j.preteyeres.2003.12.001.
8. Reichenbach, A., and Bringmann, A. (2020). Glia of the human retina. Glia *68*, 768–796. https://doi.org/10.1002/glia.23727.
9. Stone, J., and Dreher, Z. (1987). Relationship between Astrocytes, Ganglion-Cells and Vasculature of the Retina. J. Comp. Neurol. *255*, 35–49. https://doi.org/10.1002/cne.902550104.
10. Paisley, C.E., and Kay, J.N. (2021). Seeing stars: Development and function of retinal astrocytes. Dev. Biol. *478*, 144–154. https://doi.org/10.1016/j.ydbio.2021.07.007.
11. Chong, R.S., and Martin, K.R. (2015). Glial cell interactions and glaucoma. Curr. Opin. Ophthalmol. *26*, 73–77. https://doi.org/10.1097/icu.0000000000000125.
12. Garcia-Bermudez, M.Y., Freude, K.K., Mouhammad, Z.A., van Wijngaarden, P., Martin, K.K., and Kolko, M. (2021). Glial Cells in Glaucoma: Friends, Foes, and Potential Therapeutic Targets. Front. Neurol. *12*, 624983. https://doi.org/10.3389/fneur.2021.624983.
13. Liu, Y.X., Sun, H., and Guo, W.Y. (2022). Astrocyte polarization in glaucoma: a new opportunity. Neural Regen. Res. *17*, 2582–2588. https://doi.org/10.4103/1673-5374.339470.
14. Zamanian, J.L., Xu, L., Foo, L.C., Nouri, N., Zhou, L., Giffard, R.G., and Barres, B.A. (2012). Genomic analysis of reactive astrogliosis. J. Neurosci. *32*, 6391–6410. https://doi.org/10.1523/JNEUROSCI.6221-11.2012.
15. Rivera, J.C., Dabouz, R., Noueihed, B., Omri, S., Tahiri, H., and Chemtob, S. (2017). Ischemic Retinopathies: Oxidative Stress and Inflammation. Oxid. Med. Cell. Longev. *2017*, 3940241. https://doi.org/10.1155/2017/3940241.
16. Rubsam, A., Parikh, S., and Fort, P.E. (2018). Role of Inflammation in Diabetic Retinopathy. Int. J. Mol. Sci. *19*. https://doi.org/10.3390/ijms19040942.
17. Livne-Bar, I., Wei, J., Liu, H.H., Alqawlaq, S., Won, G.J., Tuccitto, A., Gronert, K., Flanagan, J.G., and Sivak, J.M. (2017). Astrocyte-derived lipoxins A4 and B4 promote neuroprotection from acute and chronic injury. J. Clin. Invest. *127*, 4403–4414. https://doi.org/10.1172/jci77398.
18. Boal, A.M., Risner, M.L., Cooper, M.L., Wareham, L.K., and Calkins, D.J. (2021). Astrocyte Networks as Therapeutic Targets in Glaucomatous Neurodegeneration. Cells *10*, 1368. https://doi.org/10.3390/cells10061368.
19. Risner, M.L., Pasini, S., Cooper, M.L., Lambert, W.S., and Calkins, D.J. (2018). Axogenic mechanism enhances retinal ganglion cell excitability during early progression in glaucoma. Proc. Natl. Acad. Sci. USA *115*, E2393–E2402. https://doi.org/10.1073/pnas.1714888115.
20. Mead, B., and Tomarev, S. (2020). Extracellular vesicle therapy for retinal diseases. Prog. Retin. Eye Res. *79*, 100849. https://doi.org/10.1016/j.preteyeres.2020.100849.
21. Cocozza, F., Grisard, E., Martin-Jaular, L., Mathieu, M., and Théry, C. (2020). SnapShot: Extracellular Vesicles. Cell *182*, 262–262.e1. https://doi.org/10.1016/j.cell.2020.04.054.
22. Kalluri, R., and LeBleu, V.S. (2020). The biology, function, and biomedical applications of exosomes. Science *367*, eaau6977. https://doi.org/10.1126/science.aau6977.
23. Tian, Y., Fu, C., Wu, Y., Lu, Y., Liu, X., and Zhang, Y. (2021). Central Nervous System Cell-Derived Exosomes in Neurodegenerative Diseases. Oxid. Med. Cell. Longev. *2021*, 9965564. https://doi.org/10.1155/2021/9965564.
24. Fan, Y., Chen, Z., and Zhang, M. (2022). Role of exosomes in the pathogenesis, diagnosis, and treatment of central nervous system diseases. J. Transl. Med. *20*, 291. https://doi.org/10.1186/s12967-022-03493-6.

25. Upadhya, R., Zingg, W., Shetty, S., and Shetty, A.K. (2020). Astrocyte-derived extracellular vesicles: Neuroreparative properties and role in the pathogenesis of neurodegenerative disorders. J. Contr. Release *323*, 225–239. https://doi.org/10.1016/j.jconrel.2020.04.017.

26. Hajrasouliha, A.R., Jiang, G., Lu, Q., Lu, H., Kaplan, H.J., Zhang, H.G., and Shao, H. (2013). Exosomes from retinal astrocytes contain antiangiogenic components that inhibit laser-induced choroidal neovascularization. J. Biol. Chem. *288*, 28058–28067. https://doi.org/10.1074/jbc.M113.470765.

27. Zhu, L., Zang, J., Liu, B., Yu, G., Hao, L., Liu, L., and Zhong, J. (2020). Oxidative stress-induced RAC autophagy can improve the HUVEC functions by releasing exosomes. J. Cell. Physiol. *235*, 7392–7409. https://doi.org/10.1002/jcp.29641.

28. Boutros, T., Chevet, E., and Metrakos, P. (2008). Mitogen-activated protein (MAP) kinase/MAP kinase phosphatase regulation: roles in cell growth, death, and cancer. Pharmacol. Rev. *60*, 261–310. https://doi.org/10.1124/pr.107.00106.

29. Hartsock, M.J., Cho, H., Wu, L., Chen, W.J., Gong, J., and Duh, E.J. (2016). A Mouse Model of Retinal Ischemia-Reperfusion Injury Through Elevation of Intraocular Pressure. J. Vis. Exp. *113*, 54065. https://doi.org/10.3791/54065.

30. Simpson, R.J., Kalra, H., and Mathivanan, S. (2012). ExoCarta as a resource for exosomal research. J. Extracell. Vesicles *1*. https://doi.org/10.3402/jev.v1i0.18374.

31. Lafourcade, C., Ramírez, J.P., Luarte, A., Fernández, A., and Wyneken, U. (2016). MIRNAS in astrocyte-derived exosomes as possible mediators of neuronal plasticity: supplementary issue: brain plasticity and repair. J. Exp. Neurosci. *10*. JEN. S39916.

32. Doyle, L.M., and Wang, M.Z. (2019). Overview of Extracellular Vesicles, Their Origin, Composition, Purpose, and Methods for Exosome Isolation and Analysis. Cells *8*, 727. https://doi.org/10.3390/cells8070727.

33. He, C., Zheng, S., Luo, Y., and Wang, B. (2018). Exosome Theranostics: Biology and Translational Medicine. Theranostics *8*, 237–255. https://doi.org/10.7150/thno.21945.

34. Molasy, M., Walczak, A., Szaflik, J., Szaflik, J.P., and Majsterek, I. (2017). MicroRNAs in glaucoma and neurodegenerative diseases. J. Hum. Genet. *62*, 105–112. https://doi.org/10.1038/jhg.2016.91.

35. Li, T., Wang, Y., Chen, J., Gao, X., Pan, S., Su, Y., and Zhou, X. (2020). Co-delivery of brinzolamide and miRNA-124 by biodegradable nanoparticles as a strategy for glaucoma therapy. Drug Deliv. *27*, 410–421. https://doi.org/10.1080/10717544.2020.1731861.

36. Ohshima, K., Inoue, K., Fujiwara, A., Hatakeyama, K., Kanto, K., Watanabe, Y., Muramatsu, K., Fukuda, Y., Ogura, S.i., Yamaguchi, K., and Mochizuki, T. (2010). Let-7 microRNA family is selectively secreted into the extracellular environment via exosomes in a metastatic gastric cancer cell line. PLoS One *5*, e13247. https://doi.org/10.1371/journal.pone.0013247.

37. Guduric-Fuchs, J., O'Connor, A., Camp, B., O'Neill, C.L., Medina, R.J., and Simpson, D.A. (2012). Selective extracellular vesicle-mediated export of an overlapping set of microRNAs from multiple cell types. BMC Genom. *13*, 357. https://doi.org/10.1186/1471-2164-13-357.

38. Tezel, G. (2022). Molecular regulation of neuroinflammation in glaucoma: Current knowledge and the ongoing search for new treatment targets. Prog. Retin. Eye Res. *87*, 100998. https://doi.org/10.1016/j.preteyeres.2021.100998.

39. Syc-Mazurek, S.B., Fernandes, K.A., and Libby, R.T. (2017). JUN is important for ocular hypertension-induced retinal ganglion cell degeneration. Cell Death Dis. *8*, e2945. https://doi.org/10.1038/cddis.2017.338.

40. Yang, J., Wu, Z., Renier, N., Simon, D.J., Uryu, K., Park, D.S., Greer, P.A., Tournier, C., Davis, R.J., and Tessier-Lavigne, M. (2015). Pathological axonal death through a MAPK cascade that triggers a local energy deficit. Cell *160*, 161–176. https://doi.org/10.1016/j.cell.2014.11.053.

41. Kimiz-Gebologlu, I., and Oncel, S.S. (2022). Exosomes: Large-scale production, isolation, drug loading efficiency, and biodistribution and uptake. J. Contr. Release *347*, 533–543. https://doi.org/10.1016/j.jconrel.2022.05.027.

42. Liang, Y., Duan, L., Lu, J., and Xia, J. (2021). Engineering exosomes for targeted drug delivery. Theranostics *11*, 3183–3195. https://doi.org/10.7150/thno.52570.

43. Zhang, Y., Bi, J., Huang, J., Tang, Y., Du, S., and Li, P. (2020). Exosome: A Review of Its Classification, Isolation Techniques, Storage, Diagnostic and Targeted Therapy Applications. Int. J. Nanomed. *15*, 6917–6934. https://doi.org/10.2147/IJN.S264498.

44. Mondal, J., Pillarisetti, S., Junnuthula, V., Saha, M., Hwang, S.R., Park, I.K., and Lee, Y.K. (2023). Hybrid exosomes, exosome-like nanovesicles and engineered exosomes for therapeutic applications. J. Contr. Release *353*, 1127–1149. https://doi.org/10.1016/j.jconrel.2022.12.027.

45. Kim, H.J., and Magrané, J. (2011). Isolation and culture of neurons and astrocytes from the mouse brain cortex. Methods Mol. Biol. *793*, 63–75. https://doi.org/10.1007/978-1-61779-328-8_4.

46. Liang, Z., Yang, L., and Lv, Y. (2021). Exosome derived from mesenchymal stem cells mediates hypoxia-specific BMP2 gene delivery and enhances bone regeneration. Chem. Eng. J. *422*. ARTN 130084. https://doi.org/10.1016/j.cej.2021.130084.

47. Rosignol, I., Villarejo-Zori, B., Teresak, P., Sierra-Filardi, E., Pereiro, X., Rodríguez-Muela, N., Vecino, E., Vieira, H.L.A., Bell, K., and Boya, P. (2020). The mito-QC Reporter for Quantitative Mitophagy Assessment in Primary Retinal Ganglion Cells and Experimental Glaucoma Models. Int. J. Mol. Sci. *21*, 1882. https://doi.org/10.3390/ijms21051882.

48. Chi, W., Li, F., Chen, H., Wang, Y., Zhu, Y., Yang, X., Zhu, J., Wu, F., Ouyang, H., Ge, J., et al. (2014). Caspase-8 promotes NLRP1/NLRP3 inflammasome activation and IL-1 beta production in acute glaucoma. Proc. Natl. Acad. Sci. USA *111*, 11181–11186. https://doi.org/10.1073/pnas.1402819111.

49. Zhang, L., Zhang, S., Yao, J., Lowery, F.J., Zhang, Q., Huang, W.C., Li, P., Li, M., Wang, X., Zhang, C., et al. (2015). Microenvironment-induced PTEN loss by exosomal microRNA primes brain metastasis outgrowth. Nature *527*, 100–104. https://doi.org/10.1038/nature15376.

50. Yang, J., Zou, T., Yang, F., Zhang, Z., Sun, C., Yang, Z., and Zhang, H. (2021). A quick protocol for the preparation of mouse retinal cryosections for immunohistochemistry. Open Biol. *11*, 210076. https://doi.org/10.1098/rsob.210076.

51. Sheng, L., Lu, B., Chen, H., Du, Y., Chen, C., Cai, W., Yang, Y., Tian, X., Huang, Z., Chi, W., et al. (2019). Marine-Steroid Derivative 5α-Androst-3β, 5α, 6β-triol Protects Retinal Ganglion Cells from Ischemia-Reperfusion Injury by Activating Nrf2 Pathway. Mar. Drugs *17*, 267. https://doi.org/10.3390/md17050267.

52. Schmittgen, T.D., and Livak, K.J. (2008). Analyzing real-time PCR data by the comparative C-T method. Nat. Protoc. *3*, 1101–1108. https://doi.org/10.1038/nprot.2008.73.